Journal of Magnetic Resonance **142,** 358–363 (2000)
doi:10.1006/jmre.1999.1955, available online at http://www.idealibrary.com on IDEAL®

Improved Reduction of Motion Artifacts in Diffusion Imaging Using Navigator Echoes and Velocity Compensation

Chris A. Clark, Gareth J. Barker, and Paul S. Tofts

NMR Research Unit, Institute of Neurology, University College London, Queen Square, London WC1N 3BG, United Kingdom

Received July 20, 1999; revised September 24, 1999

Navigator echoes provide a means with which to remove motion artifacts from diffusion-weighted images obtained using any multishot imaging technique. However, residual motion artifact is often present in the corrected images rendering the technique unreliable. It is shown that velocity-compensated diffusion sensitization when used in tandem with a navigator echo further reduces the degree of residual motion artifacts present in the corrected images and improves the reliability and clinical utility of the technique. This is demonstrated by applying a method for quantification of motion artifact to brain images of healthy volunteers scanned using both conventional (Stejskal–Tanner) and velocity-compensated gradient sensitization. Other factors affecting the efficacy of the navigator echo technique, such as brain pulsatile motion, gradient *b* factor, and navigator echo signal-to-noise ratio, are also discussed.

Key Words: **diffusion; motion; artifacts; navigator echoes; MRI.**

INTRODUCTION

Diffusion imaging is a magnetic resonance technique that provides tissue contrast that is dependent on the motion of water molecules randomly diffusing in the presence of an applied field gradient (*1–3*). The interaction between the diffusing water molecules and the local cellular structure is widely held to be an important mechanism responsible for the phenomenon of directionally dependent (anisotropic) diffusion, observed, for example, in the white matter of the human brain (*4, 5*). Thus, diffusion imaging may be used to investigate *in vivo* the structural integrity and orientation of not only healthy tissue but also diseased or injured tissue in which some modification of these water diffusion characteristics may be expected (*6–11*). In the early years of development, however, diffusion-weighted images (DWIs) obtained with spin-echo sequences suffered from severe motion artifacts rendering them radiologically redundant. Artifacts arising from bulk subject motion during the application of large diffusion sensitizing gradients induce a phase shift in each of the acquired echoes according to

$$\Delta\phi = \gamma \int \mathbf{G} \cdot \mathbf{r}\, dt, \qquad [1]$$

where **G** is the field gradient vector, **r** is a displacement vector, and γ is the gyromagnetic ratio. The subsequent disruption of the phase information in each echo causes the signal intensity to be distributed along the phase-encoding axis subsequent to Fourier transformation (FT). The magnitude reconstructed image often has a ghost-like appearance; an example is shown in Fig. 1. The dot product in Eq. [1] indicates that the phase error arises from components of motion along the direction of the applied field gradient **G**.

The principle of the navigator technique, originally described by Ehman and Felmlee (*12*) and first applied to the correction of motion artifact in DWIs by Ordidge *et al.* (*13*), is to measure and remove this phase shift from each of the acquired echoes. This can be achieved by acquiring a second (navigator) echo, following the initial imaging echo, in which the phase encoding is rewound so that the echo phase change between successive navigator echoes is dependent only on the phase change due to motion between them according to Eq. [1]. Ordidge *et al.* demonstrated that correction of the image echo phase by reversal of the motion-induced phase error measured by the navigator echo prior to 2DFT can be used to remove motion artifact due to translational rigid body motion.

Anderson and Gore (*14*) subsequently demonstrated that the correction procedure may be derived from and applied to the navigator and image echo projections, respectively, following FT along the read direction, to additionally correct for artifacts induced by rotational rigid body motion. A similar approach was described by de Crespigny *et al.* (*15*). The effect of subject rotation is to cause a shift of the echo in *k* space or equivalently induce a phase gradient or roll across the projection. In summary, six rigid body phase errors are possible, three translational ϕ_x, ϕ_y, ϕ_z and three rotational dk_x, dk_y and dk_z, where *x*, *y* and *z* represent the read, phase, and slice-select directions, respectively.

The method of Anderson and Gore can be used to correct ϕ_x, ϕ_y, ϕ_z, and dk_x while the through-plane rotational phase error dk_z may be assumed to be negligible compared to the in-plane rotational phase errors. However, the in-plane rotational phase error dk_y is not correctable using a single navigator echo. This is because the phase error in this case is restricted to the phase encode direction, whereas the navigator echo is read out along

1090-7807/00 $35.00

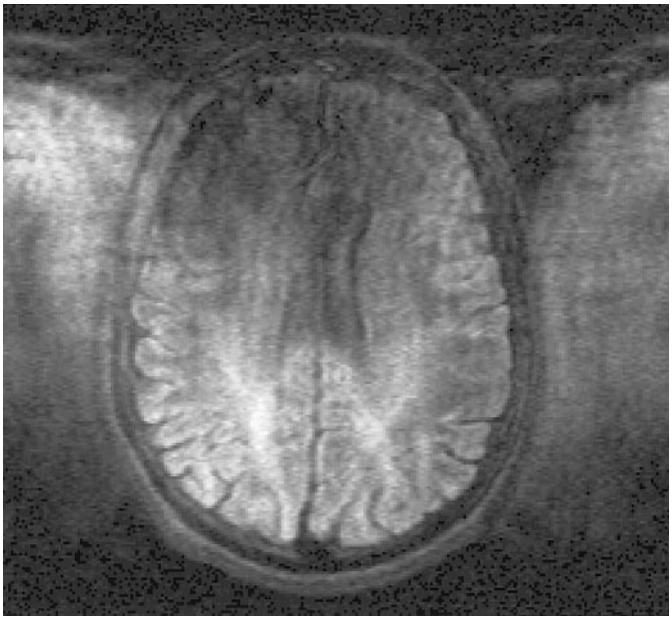

FIG. 1. Ghosting caused by shot-to-shot phase shifts.

an axis which is orthogonal to the phase direction (*14*). The dk_y phase error may be avoided by applying diffusion sensitization only along the phase direction. However, correction of dk_y may often be necessary for techniques which require sensitization in multiple directions as, for example, is required for estimation of the effective self-diffusion tensor (*16*). In this case correction of dk_y may be achieved by estimating the 2D shift of the navigator echo in *k* space by using a spiral readout scheme (*17, 18*) or by a second orthogonal navigator echo (*19*) if the imaging sequence is sufficiently rapid.

Phase errors due to constant velocity may be eliminated by use of velocity-compensated diffusion sensitization (*20*). This paper describes how the use of such gradients in tandem with a 1D navigator echo correction can be used to improve the efficiency and reliability of motion artifact removal in multishot diffusion imaging. The effect of using velocity compensation in navigated diffusion imaging is described under Theory. By defining a method for quantification of motion artifact in DWIs it is demonstrated that the mean residual artifact in navigated DWIs of 10 healthy volunteers is less with velocity-compensated gradient sensitization than with conventional (Stejskal–Tanner) (*21*) sensitization.

THEORY

Anderson and Gore (*14*) identified the combinations of diffusion sensitization direction and axis of rotation that result in a linear phase variation along the phase-encode direction dk_y. This occurs, for example, in the case of a rotation about the slice-select axis in the presence of diffusion sensitization in the readout direction. In this section we show that the use of velocity-compensated diffusion gradients can be used to reduce phase errors prior to navigation and can eliminate the linear phase variation dk_y, provided that the component of motion in the direction of diffusion sensitization is first order.

Consider the model described by Weeden *et al.* (*22*) of a disc rotating about the slice-select axis in the presence of a diffusion sensitizing gradient in the readout direction (see also Anderson and Gore (*14*)). The rotation causes a linear phase variation in a direction perpendicular to the rotation axis and gradient direction as shown in Fig. 2.

Spins will accumulate phase in proportion to their velocity component in the read direction. In this case the velocity component in the read direction is a linear function of position so that

$$v_x = \omega y. \qquad [2]$$

The phase accumulation is given by

$$dk_y = \gamma v_x \int_0^{TE} G_x t\, dt = \gamma \omega y \int_0^{TE} G_x t\, dt. \qquad [3]$$

It can be seen from this equation that the phase accumulation is proportional to the *y* position and so produces a linear phase gradient in the phase-encode direction. If velocity-compensated diffusion sensitizing gradients are used the first moment of the gradient (the integral in Eq. [3]) is zero so that $dk_y = 0$. Thus, velocity compensation can be used to reduce or, in the case of first-order motion, completely eliminate the dk_y phase errors. In addition to this, although we may expect the 1D navigator to correct for the translational phase shifts ϕ_x, ϕ_y, ϕ_z, and the rotational phase error dk_x, they will also all be zero

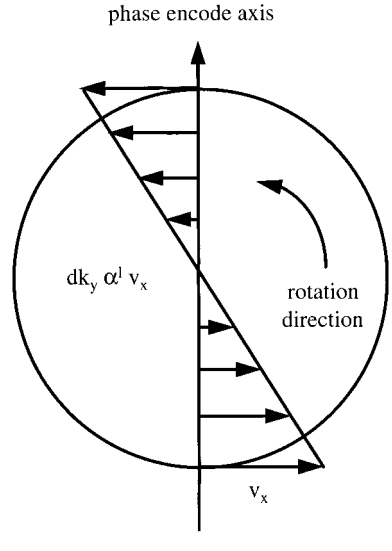

FIG. 2. Linear phase gradient in the phase-encode direction.

TABLE 1

Translational and Rotational Phase Errors That Are Corrected (✓c), Suppressed (✓s), and Remain Uncorrected/Unsuppressed (✗) Using the Navigated ST-DWI and VC-DWI Sequences

	ST-DWI		VC-DWI	
Motion	First order	Higher order	First order	Higher order
Translation ϕ_x	✓c	✓c	✓s	✓c
Translation ϕ_y	✓c	✓c	✓s	✓c
Translation ϕ_z	✓c	✓c	✓s	✓c
Rotation dk_x	✓c	✓c	✓s	✓c
Rotation dk_y	✗	✗	✓s	✗
Rotation dk_z	Negligible	Negligible	✓s	Negligible

Note. x, y, and z correspond to the read, phase, and slice-select directions, respectively.

prior to correction in the case of first-order translational and rotational motion. A summary of the possible phase errors and their elimination and correction with a navigated diffusion sensitized sequence with (i) velocity compensation (VC-DWI) and (ii) with conventional (Stejskal–Tanner) gradients (ST-DWI) is given in Table 1.

METHOD

Quantification of Residual Motion Artifact

In order to assess the effectiveness of motion artifact suppression and correction schemes it is necessary to develop a method for quantifying the degree of residual artifact remaining (if any) following correction. In the case of diffusion imaging of the brain, the signal may be distributed along the phase-encoding direction into areas of the image corresponding to air. Thus, measurement of the mean signal in the air may be used to quantify the degree of motion artifact in the magnitude DWI.

Assuming that motion artifact in DWIs is distributed uniformly across the field of view, motion artifact may be quantified in practice by manually masking out the brain and measuring the mean residual signal in the complete field of view. Thus, the mean residual signal in DWIs and images acquired in the absence of diffusion sensitization may then be compared.

If S_d is the mean background signal in a given DWI and S_0 the mean background signal in the corresponding image without diffusion sensitization then an artifact ratio (AR) may be defined as

$$\mathrm{AR} = \frac{S_d - S_0}{S_0} \qquad [4]$$

for a given slice. A DWI with AR = 0 contains no more artifact than the corresponding unweighted image. If AR $>$ 0 there is residual motion artifact in the image. A similar approach to the monitoring of motion artifact in multishot diffusion sensitized echo planar images has been described by Robson *et al.* (*23*).

Residual Motion Artifact in Navigated ST-DWIs and VC-DWIs

All measurements were performed on a whole-body 1.5-T MRI system (Signa, General Electric Medical Systems, Milwaukee, WI) equipped with actively shielded magnetic field gradients of up to 22 mT m^{-1}. A quadrature head coil of approximately 300-mm diameter was used both for RF transmission and for reception of the NMR signal.

ST-DWIs and VC-DWIs were acquired using a diffusion sensitized spin-echo sequence in the axial plane of the brain in 10 healthy volunteers with unipolar and bipolar gradient pulses positioned either side of the 180° refocusing pulse in each case. Four slices were positioned to include the basal ganglia and ventricles. The following imaging parameters were used for both ST-DWI and VC-DWI: image echo time TE_I = 100 ms, navigator echo time TE_N = 114 ms, b = 342 s mm^{-2} (using the maximum gradient strength available = 22 mT m^{-1}), 128 × 256 matrix, square 24-cm field of view and 5-mm slice thickness with a 1-mm slice gap. Thus, it was ensured that the same diffusion sensitivity and signal-to-noise ratio (SNR) for the image and navigator echoes were obtained for both ST-DWI and VC-DWI. The duration and separation of the diffusion sensitizing pulses were 21 and 29.4 ms, respectively, for ST-DWI and 19 and 20 ms, respectively, for VC-DWI. Phase encoding was in the left–right (LR) direction, readout along the anterior–posterior (AP) direction, and slice-select along the superior–inferior (SI) direction.

Following acquisition of an image in the absence of diffusion sensitization, the diffusion sensitizing gradients were applied on each gradient axis in turn. Peripheral gating was used and image acquisition was triggered from every second R-wave, monitored using a pulse oximeter on the finger. The minimum trigger delay was used so that slices 1 and 2 were acquired 13 ms after the R-wave and slices 3 and 4 acquired 135 ms after the R-wave (slices 1 and 3 are acquired after the same R-wave, slices 2 and 4 after the next R-wave). Fat saturation was used to suppress high signal from the scalp (containing subcutaneous fat) which may potentially be ghosted as a result of patient motion (a standard procedure for multishot diffusion imaging in our laboratory). A standard chin strap and padding, provided by the manufacturer, were used to restrain subjects. Imaging time was approximately 16 min per sequence, depending on heart rate. Motion artifact was then corrected off line as described by Anderson and Gore (*14*) following transfer of the raw data to a Sun workstation.

In order to investigate the relative magnitudes of motion artifacts in the ST-DWIs and VC-DWIs with sensitization along each of the gradient axes and at the two acquisition time points within the cardiac cycle, the AR was determined in the

TABLE 2

Artifact Ratio in ST-DWI before Navigation (AR_{RAW}) and after Navigation (AR_{ST}) and in VC-DWIs after Navigation (AR_{VC}) for Each Direction of Sensitization Averaged over 10 Volunteers and Four Slice Positions

Gradient axis of sensitization	AR_{RAW}	AR_{ST}	AR_{VC}
Read (AP)	0.79 ± 0.11	0.80 ± 0.12	0.62 ± 0.12
Phase (LR)	1.36 ± 0.19	0.87 ± 0.12*	0.62 ± 0.09
Slice (SI)	2.27 ± 0.19	0.89 ± 0.11*	0.59 ± 0.09**
Mean	1.47 ± 0.13	0.86 ± 0.09*	0.61 ± 0.09**

Note. The error quoted is the standard error of the mean. *$P < 0.05$ comparing AR_{RAW} and AR_{ST}. **$P < 0.05$ comparing AR_{ST} and AR_{VC}.

TABLE 3

Artifact Ratio in ST-DWI before Navigation (AR_{RAW}) and after Navigation (AR_{ST}) and in VC-DWIs after Navigation (AR_{VC}) at Two Time Points in the Cardiac Cycle Corresponding to TD = 13 ms and TD = 135 ms Averaged over 10 Volunteers and Four Slice Positions

	TD = 13 ms	TD = 135 ms
AR_{RAW}	1.89 ± 0.22	1.06 ± 0.08*
AR_{ST}	1.02 ± 0.13	0.69 ± 0.07*
AR_{VC}	0.81 ± 0.09	0.41 ± 0.08*

Note. The error quoted is the standard error of the mean. *$P < 0.001$ comparing AR at TD = 13 ms and TD = 135 ms.

corresponding navigated images and denoted AR_{ST} and AR_{VC}, respectively. In order to characterize residual motion artifact prior to navigation, AR was determined in the uncorrected ST-DWI and denoted AR_{RAW}. It is assumed that patient motion and motion artifact is a random process that obeys a normal distribution. Comparison of ARs was made using the paired two-tailed Student *t* test.

RESULTS

All results are averaged over the 10 volunteers. For each gradient axis of sensitization AR_{VC} was less than AR_{ST} although this only reached statistical significance for sensitization in the slice-select direction (Table 2). Similar levels of AR_{VC} were obtained with sensitization along each of the three gradient axes and there was an overall, statistically significant reduction in AR of 29% in the navigated VC-DWI compared to the navigated ST-DWI. Typical navigated VC-DWIs with sensitization in the read, phase, and slice-select directions are shown in Fig. 3. AR_{RAW}, AR_{ST}, and AR_{VC} averaged over the three axes of sensitization were all significantly reduced in slices acquired with TD = 135 ms compared to those acquired with TD = 13 ms (Table 3).

DISCUSSION

The results indicate that velocity-compensated diffusion sensitization further reduces residual motion artifacts in navigated DWIs compared to those acquired with conventional Stejskal–Tanner sensitization. The possible phase errors for each direction of sensitization and the corresponding reduction in AR are shown in Table 4. In particular AR was found to be reduced by 34% with sensitization along the slice-select axis, by 29% along the phase axis, and by 23% along the read axis. A possible explanation for this observation with sensitization

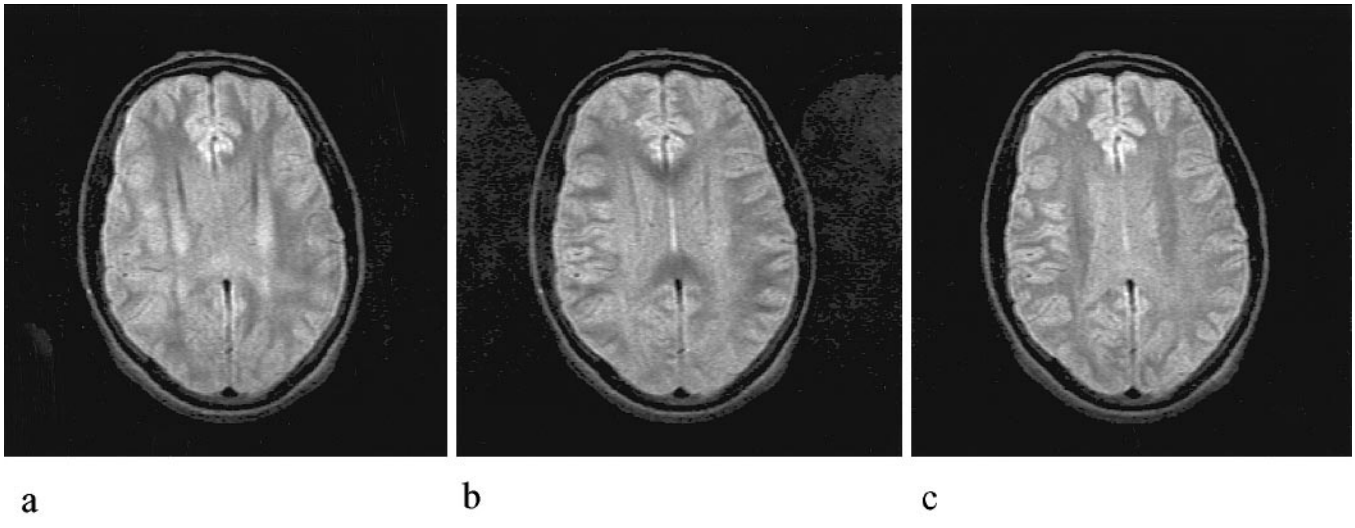

FIG. 3. Navigated VC-DWIs with sensitization along the (a) read, (b) phase, and (c) slice-select directions, respectively, with the gray level increased to reveal background signal in the air. Residual motion artifact is visible in (b) which appears as a low-intensity reconstruction of the brain but shifted by half the field of view in the phase-encode direction.

TABLE 4

Reduction in AR Attributed to Reduction in Translational and Rotational Phase Errors (Ghosting Due to dk_z Assumed Negligible)

Gradient axis of sensitization	AR_{RAW}-AR_{ST} (%)	AR_{ST}-AR_{VC} (%)	Translational phase errors	Rotational phase errors
Read (AP) G_x	−1	23	ϕ_x	dk_y
Phase (LR) G_y	36	29	ϕ_y	dk_x
Slice (SI) G_z	61	34	ϕ_z	dk_x,dk_y

Note. All but the dk_y phase errors are correctable.

along the slice-select and read axes is that the rotational phase error dk_y is significantly reduced with velocity compensation as described under Theory.

In addition, phase errors caused by nonrigid body pulsatile motion associated with the cardiac cycle in each direction may be reduced with velocity compensation. This type of phase error is not addressed by either 1D or 2D navigator echo methods. The influence of pulsatile brain motion is further underlined in the results shown in Table 3 which indicate that residual motion artifact is reduced in DWIs acquired at TD = 135 ms compared to those acquired at TD = 13 ms. These findings would appear to be in accordance with those of Wirestam *et al.* (*24*), which demonstrated that signal loss and overestimation of the diffusion coefficient resulted when TD coincided with high brain velocity. Brain parenchyma motion associated with the cardiac cycle may be demonstrated using MR phase velocity imaging (*25*). Thus, optimum TDs which coincide with the null-point of brain pulsatile motion may be identified in order to further reduce residual motion artifacts in DWIs.

ST-DWIs and VC-DWIs were acquired with the same *b* factor and echo time in order to ensure that the same navigator echo SNR was obtained for each of the sequences. It should be noted, however, that for ST-DWIs the echo time may be reduced compared to that used for VC-DWIs while maintaining the same *b* factor in order to improve SNR. It is likely that SNR may influence the performance of the navigator echo correction. One would expect errors in the estimated navigator phase to increase as SNR decreases. However, precise details of the relationship between navigator echo correction performance and SNR are unknown.

Strikingly different levels of motion artifact were observed in ST-DWIs with sensitization along each of the gradient axes prior to navigation (Table 2). The highest AR_{RAW} occurred with diffusion sensitization in the slice-select (SI) direction followed by the phase encode (LR) direction and read (AP) direction. These were all significantly different from one another ($P < 0.017$ in all cases). It is interesting to note that AR was effectively unchanged by the use of navigation in ST-DWIs with sensitization along the read (AP) axis (Table 4). In this case the correctable phase error arises from a translation along the read (AP) axis. The negligible change in AR indicates that this phase error is small, which seems reasonable given that this motion would involve the subject's head being lifted against the force of gravity and is an unlikely source of involuntary motion.

Although AR_{RAW} is highest with sensitization along the slice-select axis, it is the most reduced of the three directions by navigation (Table 4). In this case the correctable phase errors involve a translation along the slice-select (SI) axis and a rotation about the phase encode (LR) axis and are likely to be facilitated by respiratory motion in the former case and rotation of the head with the back of the head as a pivot (a nodding motion) in the latter case. Rotations about the other axes are likely to be more restricted by the foam padding.

The presence of residual artifact in navigated DWIs has implications for the choice of the optimal *b* factor that maximizes the SNR in the calculated ADC map. For estimation of the apparent diffusion coefficient (ADC) from two images with sensitization b_1 and b_2 with $b_1 < b_2$ and ignoring T_2 relaxation the fractional noise in the ADC map is given by (*26*)

$$\frac{\sigma_{ADC}}{ADC} = \frac{\sqrt{1 + e^{2b \cdot ADC}}}{b \cdot ADC \cdot SNR_0}, \qquad [5]$$

where $b = b_2 - b_1$ and SNR_0 is the SNR of the image in the absence of diffusion sensitization. This function has a flat minimum at $b \cdot ADC = 1.11$. For typical ADC values in brain white matter of 0.7×10^{-3} mm^2 s^{-1} (*5*) and $SNR_0 = 100$ the fractional noise in the ADC map is 2.9% at the optimum *b* factor $b_{opt} \sim 1500$ s mm^{-2} (assuming $b_1 = 0$ s mm^{-2}).

However, as the *b* factor is increased so is motion sensitivity and one would expect residual artifact to also increase (due to phase errors that are not correctable by navigation or suppressed by velocity compensation). Thus, an additional error in the ADC, due to residual motion artifact, should be considered. A *b* factor less than that predicted by minimum noise propagation may be more appropriate. For example the *b* factor may be reduced from its optimum value predicted by minimum noise propagation by 50% increasing the fractional noise in the ADC to only 3.7%. Although one would expect the error due to the presence of residual motion artifact to decrease in this instance the empirical relationship between residual motion artifact and *b* factor is not known but may be established through further study.

CONCLUSIONS

This study has demonstrated that residual motion artifact may be further reduced by use of velocity-compensated gradient sensitization as opposed to conventional (Stejskal–Tanner) sensitization in navigated DWIs. In principle this technique may be also be used in conjunction with echo planar multishot sequences with 1D or 2D navigation by reducing phase errors

prior to correction. We propose the use of this technique in multishot diffusion imaging to improve the accuracy and reliability of DWIs for both qualitative and quantitative clinical studies.

ACKNOWLEDGMENTS

The NMR Research Unit is funded by a generous grant from the Multiple Sclerosis Society of Great Britain and Northern Ireland. During the course of this work CAC was funded by the Brain Research Trust. CAC thanks Adam Anderson for provision of the navigator echo correction software.

REFERENCES

1. D. Le Bihan and E. Breton, Imagerie de diffusion par in vivo resonance magnetic nucleaire, *C. R. Acad. Paris* **301,** 1109–1112 (1985).
2. D. G. Taylor and M. C. Bushell, The spatial mapping of translational diffusion coefficients by the NMR imaging technique, *Phys. Med. Biol.* **30,** 345–349 (1985).
3. K. D. Merboldt, W. Hanicke, and J. Frahm, Self-diffusion NMR imaging using stimulated echoes, *J. Magn. Reson.* **64,** 479–486 (1985).
4. D. Chien, R. B. Buxton, K. K. Kwong, T. J. Brady, and B. R. Rosen, MR diffusion imaging of the human brain, *J. Comp. Assist. Tomogr.* **14,** 514–520 (1990).
5. C. Pierpaoli, P. Jezzard, P. J. Basser, A. Barnett, and G. Di Chiro, Diffusion tensor MR imaging of the human brain, *Radiology* **201,** 637–648 (1996).
6. H. L. Lutsep, G. W. Albers, A. de Crespigny, G. N. Kamat, M. P. Marks, and M. E. Moseley, Clinical utility of diffusion-weighted magnetic resonance imaging in the assessment of ischemic stroke, *Ann. Neurol.* **41,** 574–580 (1997).
7. K. Krabbe, P. Gideon, P. Wagn, U. Hansen, C. Thomsen, and F. Madsen, MR diffusion imaging of human intracranial tumours, *Neuroradiology* **39,** 483–489 (1997).
8. D. J. Werring, C. A. Clark, G. J. Barker, A. J. Thompson, and D. H. Miller, Diffusion tensor imaging of lesions and normal appearing white matter in multiple sclerosis, *Neurology* **52,** 1626–1632 (1999).
9. U. C. Wieshmann, C. A. Clark, M. R. Symms, G. J. Barker, K. D. Birnie, and S. D. Shorvon. Water diffusion in the human hippocampus in epilepsy, *Magn. Reson. Imaging* **17,** 29–36 (1999).
10. M. M. Bahn, D. K. Kido, W. Lin, and A. L. Pearlman, Brain magnetic resonance diffusion abnormalities in Creutzfeldt–Jakob disease, *Arch. Neurol.* **54,** 1411–1415 (1997).
11. D. J. Werring, C. A. Clark, G. J. Barker, D. H. Miller, G. J. M. Parker, M. J. Brammer, E. T. Bullmore, V. P. Giampietro, and A. J. Thompson, The structural and functional mechanisms of motor recovery: Complementary use of diffusion tensor and functional magnetic resonance imaging in a traumatic injury of the internal capsule, *J. Neurol. Neurosurg. Psychol.* **65,** 863–869 (1998).
12. R. L. Ehman and J. P. Felmlee, Adaptive technique for high definition MR imaging of moving structures, *Radiology* **173,** 255–263 (1989).
13. R. J. Ordidge, J. A. Helpern, Z. Q. Qing, R. A. Knight, and V. Nagesh, Correction of motional artifacts in diffusion-weighted MR images using navigator echoes, *Magn. Reson. Imaging* **12,** 455–460 (1994).
14. A. W. Anderson and J. C. Gore, Analysis and correction of motion artifacts in diffusion weighted imaging, *Magn. Reson. Med.* **32,** 379–387 (1994).
15. A. de Crespigny, M. P. Marks, D. R. Enzmann, and M. E. Moseley, Navigated diffusion imaging of normal and ischemic human brain, *Magn. Reson. Med.* **33,** 720–728 (1995).
16. P. J. Basser, D. Le Bihan, and J. Mattiello, Estimation of the effective self-diffusion tensor from the NMR spin echo, *J. Magn. Reson. B* **103,** 247–254 (1994).
17. A. W. Anderson and J. C. Gore, Using spiral navigator echoes to correct for motion in diffusion weighted imaging, *In* "Proceedings of the Third Scientific Meeting, Society of Magnetic Resonance," p. 743, Nice, France (1995).
18. K. Butts, J. Pauly, A. de Crespigny, and M. Moseley, Isotropic diffusion-weighted and spiral-navigated interleaved EPI for routine imaging of acute stroke, *Magn. Reson. Med.* **38,** 741–749 (1997).
19. K. Butts, A. de Crespigny, J. M. Pauly, and M. Moseley, Diffusion-weighted interleaved echo-planar imaging with a pair of orthogonal navigator echoes. *Magn. Reson. Med.* **35,** 763–770 (1996).
20. C. Thomsen, P. Ring, and O. Henriksen, In vivo measurement of water self diffusion by magnetic resonance imaging, *In* "Proceedings of the Seventh Scientific Meeting, Society of Magnetic Resonance in Medicine," p. 890, San Francisco, CA (1988).
21. E. O. Stejskal and J. E. Tanner, Spin diffusion measurements: Spin echoes in the presence of a time-dependent field gradient, *J. Chem. Phys.* **42,** 288–292 (1965).
22. V. J. Weeden, R. M. Weisskoff, and B. P. Poncelet. MRI signal void due to in-plane motion is all or none. *Magn. Reson. Med.* **32,** 116–120 (1994).
23. M. D. Robson, A. W. Anderson, and J. C. Gore. Diffusion-weighted multiple shot echo planar imaging of humans without navigation. *Magn. Reson. Med.* **38,** 82–88 (1997).
24. R. Wirestam, D. Greitz, C. Thomsen, S. Brockstedt, M. B. E. Olsson, and F. Stahlberg, Theoretical and experimental evaluation of phase-dispersion effects caused by brain motion in diffusion and perfusion MR imaging, *J. Magn. Reson. Imaging* **6,** 348–355 (1996).
25. B. P. Poncelet, V. J. Weeden, R. M. Weisskoff, and M. S. Cohen, Brain parenchyma motion: Measurement with cine echo-planar MR imaging, *Radiology* **185,** 645–651 (1992).
26. P. V. Prasad and O. Nalcioglu, A modified pulse sequence for in vivo diffusion imaging with reduced motion artifacts, *Magn. Reson. Med.* **18,** 116–131 (1991).